



OPEN

Stress-dependent Mohr–Coulomb shear strength parameters for intact rock

Hao Li¹, Leo Pel², Zhenjiang You^{3,4,5} & David Smeulders¹

Rock strength is imperative for the design and stability analysis of engineering structures. The Mohr–Coulomb (M-C) criterion holds significant prominence in geotechnical engineering. However, the M-C criterion fails to accurately capture the nonlinear strength response and neglects the critical state of rocks, potentially leading to inaccuracies in the design phase of deep engineering projects. This study introduces an innovative stress-dependent friction angle and cohesion (SFC) for the M-C criterion to capture the nonlinear strength responses of intact rocks, spanning from non-critical to critical states (brittle to ductile regions). A novel method for determining these stress-dependent parameters at each corresponding σ_3 is initially introduced. Subsequently, an examination of the confinement dependency of the friction angle and cohesion is conducted, leading to the derivation of the SFC model. The SFC-enhanced M-C criterion, utilizing parameters obtained from triaxial tests under lower σ_3 , demonstrates the capability to delineate the complete non-linear strength envelope from brittle to ductile regions. Validation through triaxial test data confirms that the predictions of the SFC-enhanced M-C criterion accurately correspond to the strength characteristics of the tested rocks.

Keywords Mohr–Coulomb (M-C) criterion, Stress-dependent cohesion and friction angle, Critical state, Brittle to ductile, Nonlinear strength envelope

In recent decades, engineering activities have extended to deeper regions^{1,2}. For example, the depth of the mining activities has reached more than 4000 m below the surface^{3,4}. As engineering constructions delve deeper underground, crustal stress intensifies, increasing the proneness of geological hazards, such as collapse⁵. Hence, accurately estimating rock strength across a broad range of confining pressures becomes the pivotal concern for deep engineering constructions.

The strength criterion predicts rock strength under specific stress conditions, which is vital for the stability and safety design of geotechnical engineering applications like tunnels, mines, and slopes. The Mohr–Coulomb (M-C) criterion is the best-known rock strength criterion. It is defined as follows:

$$\sigma_1 = \tan^2 \left(\frac{\pi}{4} + \frac{\phi}{2} \right) \sigma_3 + 2c \tan \left(\frac{\pi}{4} + \frac{\phi}{2} \right) \quad (1)$$

where c and ϕ are the cohesion and friction angle.

Despite its widespread use in industry, the classical M-C criterion fails to capture the nonlinear compressive strength response of rocks under various confining pressures and neglects the critical state. These deficiencies may potentially lead to inaccuracies in stability analysis for deep engineering projects. Figure 1 reproduces Mogi's data⁶. It shows the convexity strength envelopes of different rocks with a steep initial slope that gradually diminishes with increasing confining pressure, eventually becoming horizontal beyond a particular point. Barton^{7,8} termed this point the critical state, where the peak deviatoric strength envelope reaches a zero gradient, with the peak deviatoric strength remaining approximately constant thereafter. In this scenario, the classical M-C criterion fails to accurately describe the strength of the material at various confining pressures, potentially yielding inaccurate results in the design of deep engineering constructions.

¹Department of Mechanical Engineering, Eindhoven University of Technology, 5600 MB Eindhoven, The Netherlands. ²Department of Applied Physics, Eindhoven University of Technology, 5600 MB Eindhoven, The Netherlands. ³School of Petroleum, China University of Petroleum-Beijing at Karamay, Karamay 834000, China. ⁴Centre for Sustainable Energy and Resources, Edith Cowan University, Joondalup, WA 6027, Australia. ⁵School of Chemical Engineering, The University of Queensland, Brisbane, QLD 4072, Australia. ✉email: haoli424@outlook.com; l.pel@tue.nl

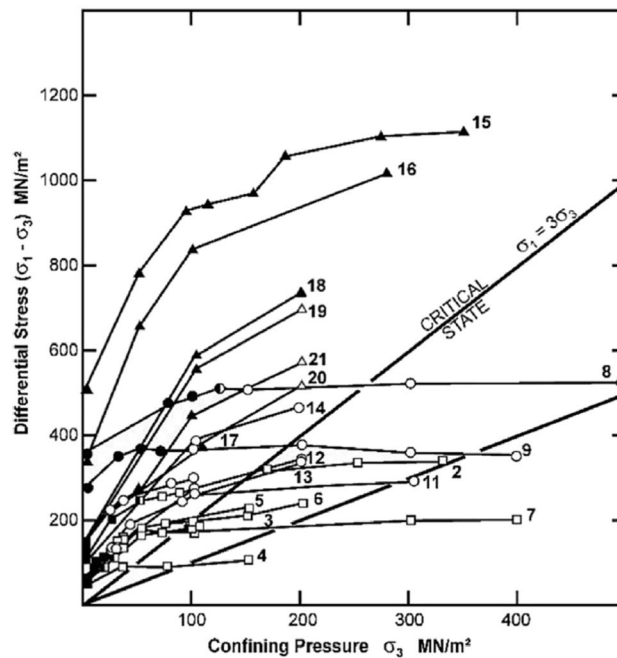


Figure 1. Triaxial data for dry carbonate rocks compiled by Mogi in his Fig. 3⁶. Brittle, brittle-ductile transitional and ductile behavior are presented by closed, half-open and open symbols, respectively. The solid line represents the critical state proposed by Barton⁷.

Several empirical equations have been developed for the nonlinear strength envelope. Power, parabolic, exponential, and logarithmic functions are employed^{9–15}. While empirical criteria based on simple fitting of experimental data demonstrate high accuracy in predicting the strength of rocks, the M-C criterion remains the most extensively utilized principle in rock mechanics. This is because it is embedded in various commercial numerical simulation codes, such as Fast Lagrangian Analysis of Continua (FLAC), as well as constitutive models for rocks. These widespread adoptions of the M-C criterion highlights its evolution into an indispensable tool for engineers and researchers. Therefore, enhancing the M-C criterion to capture the nonlinear strength responses of intact rocks spanning from non-to-critical states is essential and could significantly contribute to the fields of geotechnical engineering.

In the pursuit of enhancing the M-C criterion to capture the nonlinear strength responses of rocks, several modified M-C criteria have been proposed by researchers. For instance, Singh et al.¹⁰ modified the classical M-C criterion using a parabolic expression. Xie et al.¹⁶ introduced an intermediate variable into the classical M-C criterion and then transformed it into a quadratic formulation. Singh et al.¹⁷ adapted the classical M-C criterion by incorporating a confining stress term based on the critical state concept. These research efforts significantly enhance the accuracy of strength determinations for rocks subjected to a broader range of confining pressures. Furthermore, introducing the equivalent friction angle and cohesion represents a robust strategy for enhancing the M-C criterion. Two widely accepted methods have been recognized to determine these equivalent parameters. The first approach is proposed by Balmer¹⁸. This method uses the tangents to the nonlinear Hoek–Brown (H-B) strength envelope at each confining or normal stress. The slope and intercept of the tangent line serve to determine these equivalent shear parameters^{19–28}. The second method, pioneered by Hoek et al.²⁹, involves determining the equivalent shear parameters by fitting an average linear segment of the nonlinear failure envelope across a specific range of confining stresses. The above approaches have garnered widespread acceptance among researchers due to their ability to comprehensively account for the nonlinear strength responses exhibited by various rock types. Moreover, the mathematical expression for the M-C criterion with equivalent shear parameters remains consistent with the classical form, albeit with the cohesion and friction angle terms now dependent on the H-B parameters. This feature facilitates seamless integration with various commercial numerical simulation codes and constitutive models for rocks. Although these two approaches are applicable, there are still two limitations: Firstly, the accuracy of these approaches relies on the range of confining stress encompassed by the experimental data used to establish the pre-determined strength envelope. Limited data at lower confining stress levels may cause both the Balmer and Hoek methods to overestimate strength at higher confining stresses, leading to inaccuracies in determining the equivalent parameters. Conducting triaxial tests covering a wide range of confining stresses is necessary to ensure accuracy, but this can be time-consuming and resource-intensive, particularly for rocks with high critical confining stresses (such as granite and marble, where the critical confining stress can exceed 400 MPa, and even reach 1000 MPa^{30,31}). Secondly, neglecting the critical state concept in the pre-determined strength envelope, even with data spanning a wide range of confining pressure, may hinder the accuracy of the entire strength prediction. This can potentially introduce inaccuracies in the determination of the equivalent parameters (to be discussed in the Discussion Section). Hence, developing a

novel methodology is crucial to address these limitations and accurately determine friction angle and cohesion across the entire stress spectrum from non-critical to critical states.

In this paper, an innovative stress-dependent friction angle and cohesion (SFC) is proposed and incorporated into the M-C criterion. A novel method for determining these parameters at each corresponding σ_3 is initially proposed, leading to the derivation of the SFC model describing their relationship with the corresponding σ_3 . The SFC-enhanced M-C criterion, using parameters acquired through triaxial tests under lower confining pressures, can project the complete non-linear strength envelope, spanning from brittle to ductile behavior. Finally, the SFC-enhanced M-C criterion's validity is substantiated through triaxial test data.

The stress-dependent cohesion (c_i) and friction angle (ϕ_i)

This section aims to quantify the ϕ_i and c_i at their corresponding σ_3 using a novel method. We then explore their stress dependency and establish the SFC model. To achieve these goals, triaxial compression test data for four types of rocks (Jinyun sandstone from our test, Solnhofen limestone³², Dazhi Marble³³ and Shanxi Mudstone³⁴) are provided in Table 1.

The specimens in our test were collected from Jinyun Mountain in China. The specimens were cylindrical (length: 100 mm, diameter: 50 mm. See Fig. 2b). Triaxial tests were conducted using the Rock Testing System with servo control capabilities. The triaxial cell of the system (Fig. 2a) has two high-pressure oil pumps, which

Rock type	Stress	Experimental data/MPa									
Jinyun sandstone	σ_3	0	2.5	5	10	20	30	40	50	60	
	σ_1	76.8	110.5	154.7	200.5	250.9	277.7	298.4	312.5	320.5	
Solnhofen limestone from Ref. ³²	σ_3	0	6	15	24	46	72	111	195	304	
	σ_1	293	335	360	381	426	467	518	595	709	
Dazhi Marble from Ref. ³³	σ_3	0	10	20	40	60	70	120	135		
	σ_1	70	107	136	183	221	237	290	305		
Shanxi Mudstone from Ref. ³⁴	σ_3	0	5	10	20	30	40	50			
	σ_1	21.53	32.75	39.85	45.45	55.55	67.25	77.33			

Table 1. Experimental data of different rock specimens.

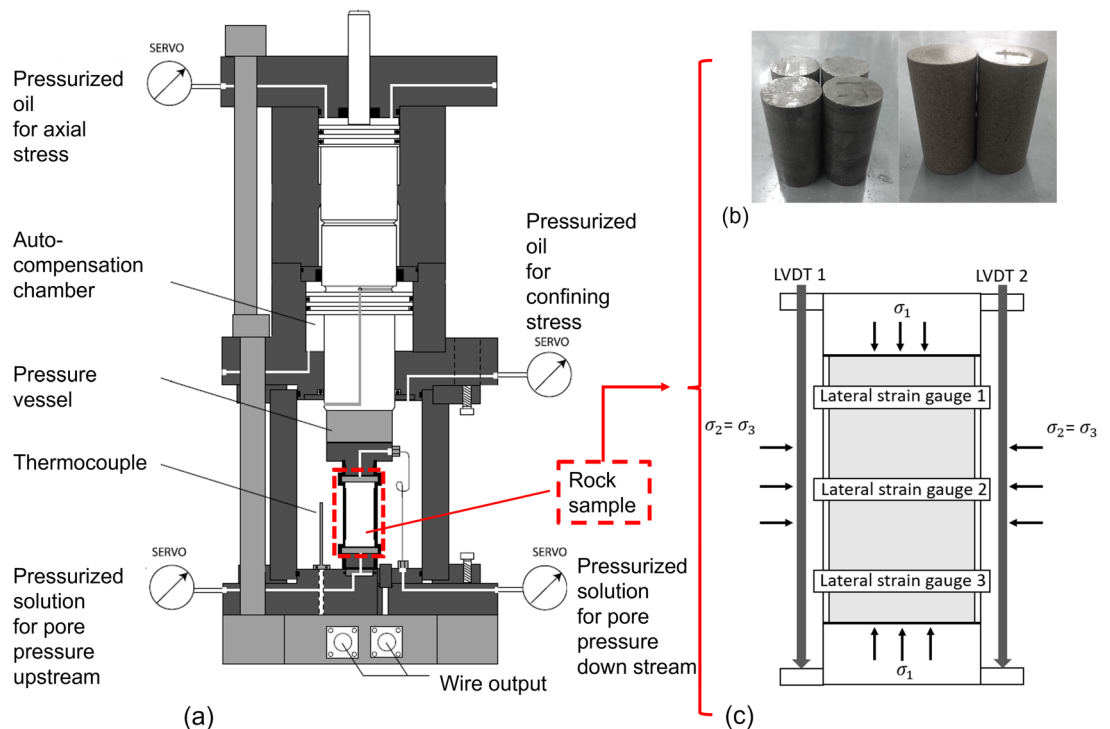


Figure 2. Rock testing facility. (a) Schematic of the triaxial cell. The axial and confining stresses are supplied and maintained by high-pressure oil pumps. (b) Photograph of cylindrical rock specimens (left: limestone specimens; right: sandstone specimens) used in laboratory tests. (c) Schematic of the specimen cell. The grey shaded part is the rock specimen. The specimen in this cell is under the isotropic lateral compression, *i.e.*, $\sigma_1 > \sigma_2 = \sigma_3$.

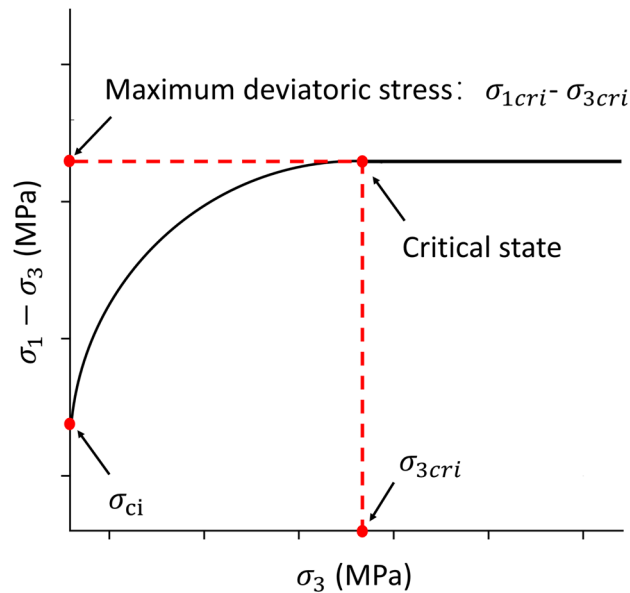


Figure 3. A representative strength responses of rock at various confining pressures, derived from Barton^{7,8}, Singh et al.¹⁷, Wang et al.³⁹, Shen et al.⁴⁰, and You⁹. σ_{ci} is the uniaxial compressive strength (UCS). σ_{3cri} and σ_{1cri} are the confining pressure and strength at the critical state.

are responsible for supplying and maintaining the axial and confining stresses. Data acquisition sensors are employed to capture stress data, including axial stress and confining stress. Figure 2c depicts the specimen cell configuration. The rock specimens are encased in polyolefin membranes with a thickness of 2 mm and positioned at the centre of the specimen cell. The axial strain is measured using two linear variable differential transformers (LVDTs) positioned at the bottom and top surfaces of the specimen, while lateral strain is monitored using three strain gauges. Triaxial compression tests were conducted with different confining stresses (see Table 1). Each compression test had two loading steps: first, σ_1 , σ_2 and σ_3 were applied with pre-set hydrostatic pressures (Loading Rate = 0.2 MPa/s). Second, σ_2 and σ_3 were maintained, while σ_1 was increased (Loading Rate = 0.02 mm/min) until the specimen failed.

The calculation of ϕ_i and c_i at each σ_3 can be achieved using the tangent of two consecutive Mohr circles^{35–38}. However, this method may produce erratic results due to scattered strength data caused by rock discreteness. This study introduces an innovative method to address this issue. A pre-established smoothed strength response is initially constructed to facilitate the subsequent determination of ϕ_i and c_i . Utilizing the data in Fig. 1 and Table 1, and guided by the critical state concept proposed by Barton^{7,8} and the research conducted by Singh et al.¹⁷, Wang et al.³⁹, Shen et al.⁴⁰, and You⁹, a representative strength responses for rock in the $(\sigma_1 - \sigma_3)$ versus (σ_3) space is depicted in Fig. 3.

Preceding the critical state, the strength response exhibits an upward convexity, reaching a horizontal peak after attaining the critical state. Leveraging the strength envelope presented in Fig. 3, a modified exponential (EXP) criterion is employed. The original version of the EXP criterion was proposed by You⁹, whose efficacy has been confirmed through validation by You⁴¹, demonstrating its capability for a favorable fit across various rock types. However, the critical state concept was not clarified in its original version. Therefore, based on the critical state concept, a modified EXP criterion is presented in Eq. (2).

$$\sigma_1 = \sigma_3 + (\sigma_{ci} - \sigma_{dcri}) \cdot \exp(\sigma_3/n_1) + \sigma_{dcri} \quad (2)$$

where n_1 is the material constant obtained by data fitting. As depicted in Fig. 3, σ_{ci} is the uniaxial compressive strength (UCS), and σ_{dcri} is the ultimate deviatoric stress ($\sigma_{1cri} - \sigma_{3cri}$) at the critical state. Note that when the triaxial data encompasses the range from the non-critical to the critical states, both the σ_{3cri} and σ_{dcri} can be directly derived from the test data. In scenarios where only test data at lower confining pressures before the critical state are accessible, σ_{3cri} and σ_{dcri} need to be pre-estimated. From the investigations on 158 sets of test data over a thousand experimental tests, it is found that σ_{3cri} is approximately equal to the UCS¹⁷. Additionally, σ_{1cri} can be determined by Byerlee's rule: $\sigma_{1cri} = 4.7\sigma_{3cri}$ ^{42,43}. Parameter n_1 is then determined by fitting a plot of σ_1 versus σ_3 using the least squares method.

The rationale for selecting the least squares method is as follows: Firstly, it is the predominant approach for data fitting within the geological engineering research field. Recommended by researchers, this method has been successfully applied to acquire parameters for strength criteria such as the M-C and H-B criteria^{44–46}. Secondly, there is only one parameter in each equation (i.e., Eqs. (2), (4a) and (4b)) that needs to be fitted. Additionally, the plot used for fitting exhibits simple concave or convex curves, rendering the least squares method adequate for achieving accurate results. Thirdly, validation in section “Model verification” will further confirm that parameters

obtained through the least squares method can be effectively utilized for strength determination, resulting in accurate strength predictions.

By utilizing the modified EXP criterion, it becomes possible to calculate ϕ_i and c_i :

$$\phi_i = 2 \cdot \left(\tan^{-1} \sqrt{\left(1 + \frac{\sigma_{ci} - \sigma_{dcri}}{n_1} \exp\left(\frac{\sigma_3}{n_1}\right) \right)} - \frac{\pi}{4} \right) \quad (3a)$$

$$c_i = \frac{\left(\sigma_1 - \tan^2 \left(\frac{\pi}{4} + \frac{\phi_i}{2} \right) \sigma_3 \right)}{2 \tan \left(\frac{\pi}{4} + \frac{\phi_i}{2} \right)} \quad (3b)$$

Utilizing Eqs. (1), (2), and (3a), (3b), the calculation process for ϕ_i and c_i unfolds as follows: first, obtain the preliminary empirical nonlinear strength responses using the modified EXP criterion (Eq. 2). Second, determine ϕ_i using Eq. (3a). Third, compute c_i using Eq. (3b). It's important to clarify that the strength data used in Steps 2 and 3 originate from the modified EXP criterion, while the ϕ_i used in Step 3 is derived from Step 2.

Utilizing the above process, the calculated stress-dependent friction angle and cohesion (black points) are plotted in Fig. 4a–h. It is observed that ϕ_i decreases and c_i increases with the increasing σ_3 . Based on Fig. 4a–h, the conceptual relations of ϕ_i and c_i with σ_3 are plotted in Fig. 4i,j, respectively. The curve of the stress-dependent friction angle is concave and eventually approaches zero at the critical state. The slope of the ϕ_i curve is steep initially, then gradually decreases with the increasing σ_3 , and finally tends to be zero. This indicates that the decreasing rate of ϕ_i decreases with increasing σ_3 . In contrast, the c_i curve is convex upward, reaching its maximum value at the critical state and becoming horizontal thereafter. Similarly, the slope of the c_i curve is steep initially and gradually decreases to zero at the critical state. Based on the observations above, the exponential function is considered the best option to capture ϕ_i and c_i at various σ_3 .

$$\phi_i = \phi_0 \exp(-\sigma_3 / \delta_\phi) \quad (4a)$$

$$c_i = (c_0 - c_u) \exp(-\sigma_3 / \delta_c) + c_{cri} \quad (4b)$$

where δ_ϕ and δ_c are material constants control the shape of ϕ_i and c_i curves. The physical significance of these parameters will be elucidated in the Discussion section. ϕ_0 is the initial value of ϕ_i , and c_0 and c_{cri} are the initial and final c_i at the critical state, respectively. Equations (4a) and (4b) constitute the Stress-dependent Friction Angle and Cohesion (SFC) model. By employing this model, it becomes possible to describe and visualize the variations in ϕ_i and c_i for the four rocks specified in Table 1. The ϕ_i and c_i described by the SFC model, along with its parameters, are graphically presented in Fig. 4 (see the red solid lines).

The mobilizations of ϕ_i and c_i relate to the rock failure mechanism. The M-C criterion considers the material strength comprises frictional and cohesive strength components. Rock, as a representative strong cohesive geomaterial, exemplifies this concept. Cohesion in rock is the molecular attraction and mobilization resistance between mineral grains, as well as the breaking resistance of bonds and cement. The frictional component, on the other hand, is related to the number, area, roughness, and degree of closure of the cracks. Rock failure is a crack (damage) development process that involves the initiation, interaction, and coalescence of microcracks, ultimately leading to the formation of macrocracks and culminating in final rupture. This damage development process often concentrates on one or more zones of the rock, referred to as damage localization⁴⁷. During the crack development and localization process, the cohesive component is gradually replaced by the frictional component. Therefore, the larger the crack area, the smaller the intact area, resulting in decreased cohesion and increased friction.

Confining stress significantly influences the final failure characteristics and brittleness of the rock, consequently impacting both the internal friction angle and cohesion. Upon compression, crack closure initiates, initially causing interlocking due to the irregularities of crack surfaces. As load increases, frictional resistance rises, restraining movement between crack surfaces. Once the axial stress surpasses a critical threshold, shear sliding occurs, leading to stable initiation of tensile cracks from pre-existing crack tips^{48,49}. At low confining pressures, normal stress perpendicular to the crack surface is low, resulting in incomplete interlocking of pore surfaces. Consequently, crack surface resistance diminishes, allowing for easier propagation of tensile cracks parallel to the axial stress direction, ultimately leading to penetration of the rock. This leads to higher fragmentation and decreased integrity of the rock, characterized by higher brightness, lower cohesion and higher friction angle. As the confinement increases, the rock's failure mode transitions from a mix of shear and tensile failure to single-shear sliding. This transition, known as the brittle-semi-brittle transition, is characterized by a reduction in both the number and volume of cracks, accompanied by an increase in the integrity of the solid parts. Consequently, the friction angle decreases while the cohesion increases. This transition rises from the following mechanisms: Elevated confining pressure results in increased normal stress and enhanced compaction of the pores⁵⁰, leading to complete interlocking of the pore surfaces and heightened sliding resistance. Consequently, the first crack propagation deviates from the axial stress direction, occurring at an angle that increases with the rising confining pressure. With further loading, these initial cracks coalesce to form a major shear band oriented at a certain angle to the axial stress direction^{51,52}. As σ_3 increases to the critical state, rock shifts from crack failure to ductile flow, specifically compactive cataclastic flow. Consequently, macro cracks do not occur, resulting in ϕ_i approaching zero and c_i attaining its maximum value.

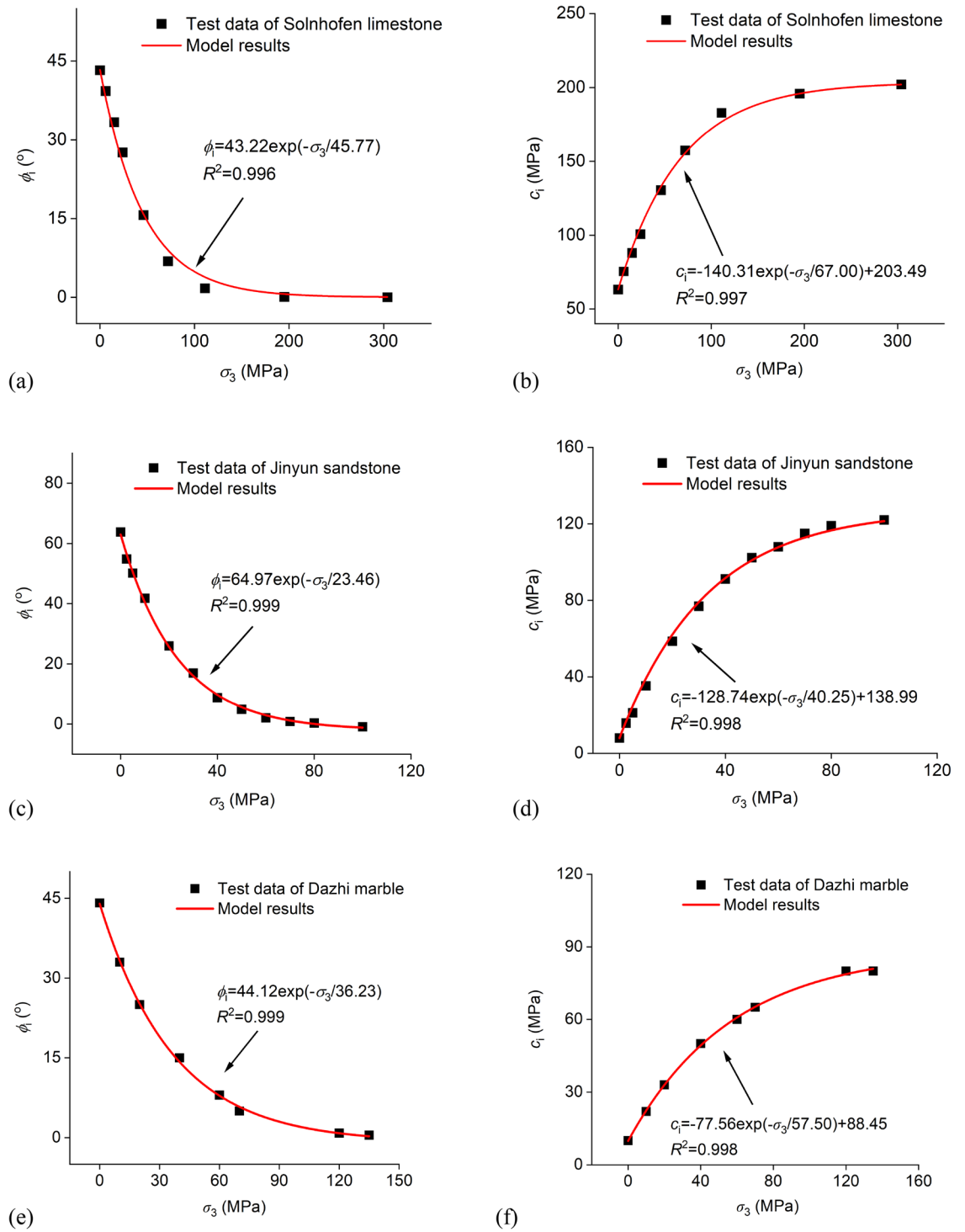


Figure 4. Stress-dependent friction angle and cohesion for experimental data in Table 1. (a, b) Friction angle and cohesion of Solnhofen limestone³². (c, d) Friction angle and cohesion of Jinyun sandstone. (e, f) Friction angle and cohesion of Dazhi Marble³³. (g, h) Friction angle and cohesion of Shanxi Mudstone³⁴. Note that the solid points represent the stress-dependent friction angle and cohesion calculated using the method presented in section “The stress-dependent cohesion (c_i) and friction angle (ϕ_i)”, while the red solid lines depict the results from the SFC model. (i) Conceptual diagram of friction angle as a function of confining stress. (j) Conceptual diagram of cohesion as a function of confining stress.

Model verification

Henceforth, the criterion incorporated with the SFC model is denoted as the “SFC-enhanced criterion”. In

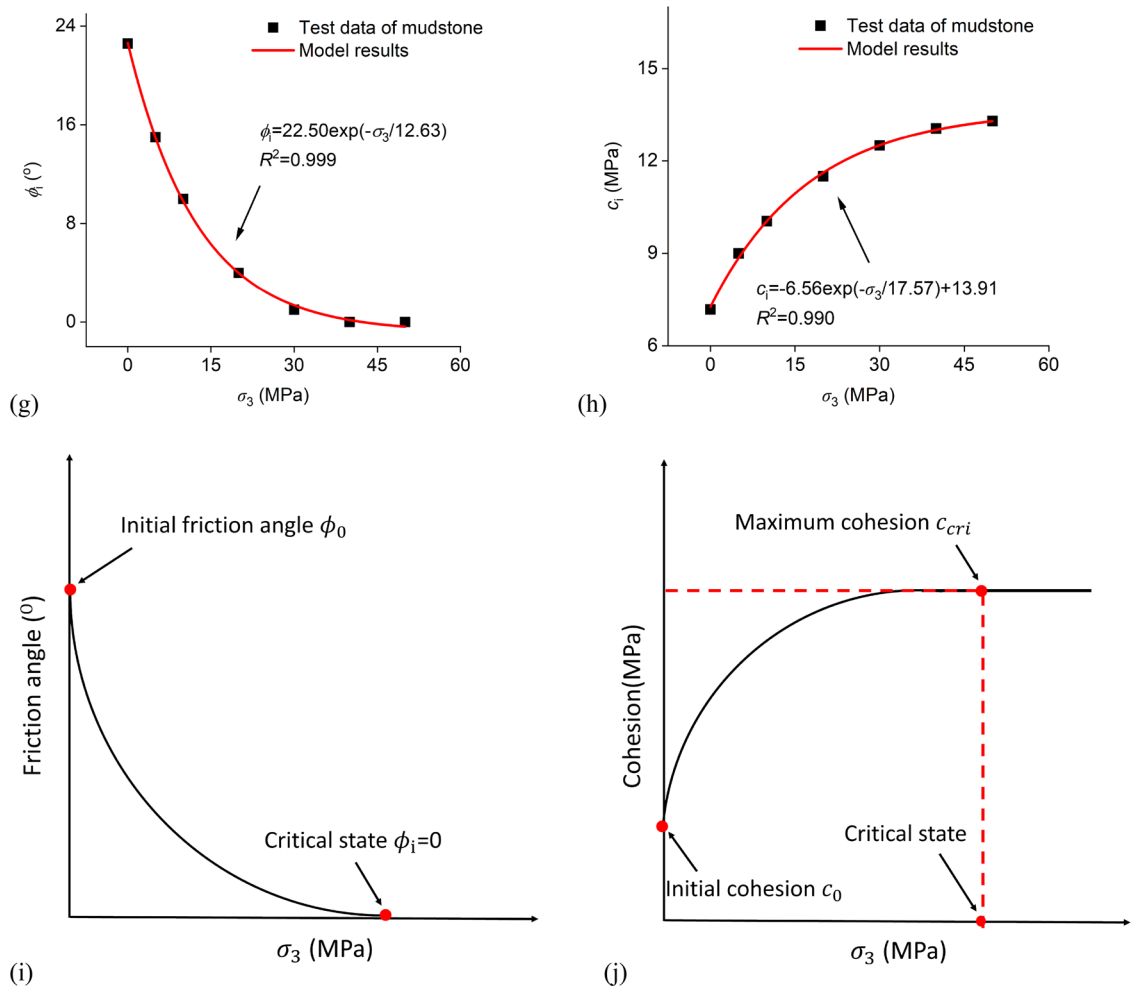


Figure 4. (continued)

contrast, its original version, featuring a constant friction angle and cohesion derived from the linear M-C criterion, is called the “classical criterion”. In this section, the performance of the SFC-enhanced M-C criterion is evaluated using data from 14 types of rocks, including the data presented in Tables 1 and 2. The procedure for determining ϕ_i and c_i is depicted in Fig. 5, outlining the following steps:

1. Build the pre-established EXP strength envelope (Eq. (2)).
2. Determining the ϕ_i equation (i.e., Eq. (4a)). ϕ_0 is determined by the tangent of two adjacent Mohr circles, which correspond to the UCS and the strength at a lower σ_3 , for instance, the strength at $\sigma_3 = 2.5$ MPa of the Jinyun limestone and sandstone data in Table 1. After that, calculate the rest ϕ_i using Eq. (3a). Note that the strength value for this calculation originates from the predictions of the EXP criterion. Finally, δ_ϕ is determined by fitting a plot of ϕ_i versus σ_3 using the least squares method.
3. Determining the c_i equation (Eq. (4b)). Similar to that of the ϕ_0 , c_0 is determined based on the UCS and the nearest strength point at the lower σ_3 . The rest c_i at every σ_3 is calculated by Eq. (3b). Note that the ϕ_i in Eq. (3b) is derived in step 2. Finally, δ_c is determined by fitting a plot of c_i versus σ_3 using the least squares method.

Following the procedural guidelines outlined in Fig. 5, the SFC-enhanced M-C criterion can be employed to assess rock strength. The test data and outcomes derived from the SFC-enhanced M-C criterion are compared in Fig. 6. Additionally, Fig. 6 furnishes the input parameters of the SFC alongside the coefficient of determination, R^2 . A higher R^2 value signifies a superior fit. Figure 6 illustrates that the enhanced M-C criterion adeptly captures the nonlinear strength envelope of intact rock at a laboratory scale, yielding higher prediction accuracy and demonstrating broader applicability across various types of rocks.

The enhanced M-C criterion incorporating stress-dependent parameters proposed in this paper applies to intact rock at a laboratory scale. It is important to emphasize that the enhanced M-C criterion, along with the methodology for determining the stress-dependent friction angle and cohesion, holds potential applicability for jointed rock masses. Research endeavours by scholars such as Barton⁸ and Singh¹⁷ have revealed that the strength envelope of jointed rock masses in the $(\sigma_1 - \sigma_3)$ versus (σ_3) space assumes a concave curve akin to that illustrated

Rock type	Stress	Experimental data/MPa										
		σ_3	σ_1	σ_2	σ_3	σ_1	σ_2	σ_3	σ_1	σ_2	σ_3	σ_1
Indiana limestone from Ref. ⁵³	σ_3	0	6.5	13.7	20.3	27.9	34.4	41.2	48.4	55.4	62.3	68.4
	σ_1	44	66	85	99	109	119	128.2	135.1	141.9	149.1	156.5
Byerlee granite from Ref. ³¹	σ_3	0	50	140	160	200	220	300	380	500	600	1000
	σ_1	480	775	1110	1205	1450	1500	1690	1900	2325	2420	2800
Jinping sandstone from Ref. ⁵⁴	σ_3	0	5	10	20	30	40	50	60	70		
	σ_1	61.6	109.5	138.6	174.6	209	240.5	263	288.5	305.4		
Nanjing sandstone from Ref. ⁴³	σ_3	0	5	10	20	30	40	50	60	70	90	120
	σ_1	75	115	145	195	240	270	295	320	340	370	410
Pingdingshan sandstone from Ref. ⁹	σ_3	0	5	10	15	20	25	30	40			
	σ_1	102	157.7	197	224.8	238	258	283	305			
Nanyang marble from Ref. ⁹	σ_3	0	5	10	20	30	40					
	σ_1	84.1	131.7	168.3	226.8	266.2	301.9					
Jinyunshan Limestone from our test	σ_3	0	5	10	20	30						
	σ_1	139.7	210.1	250.5	321.4	360.1						
Dunham dolomite from Ref. ⁵⁵	σ_3	0	25	45	60	65	85	105	125			
	σ_1	262	400	487	540	568	620	682	725			
Yamaguchi marble from Ref. ³²	σ_3	0	6	12.5	25	40	55	70	85	100	150	200
	σ_1	81	113	130	175	210	246	272	295	324	397	454
Dun Mountain dunite from Ref. ⁵⁶	σ_3	0	55	137	250	340	435	490	770	1000	1270	1500
	σ_1	190	724	1187	1630	1970	2375	2510	3260	4190	3900	4700
	σ_3	1990	2010	2500	2750	3000						
	σ_1	5460	5100	6250	6330	7040						

Table 2. Triaxial test data of different rocks for model verification.

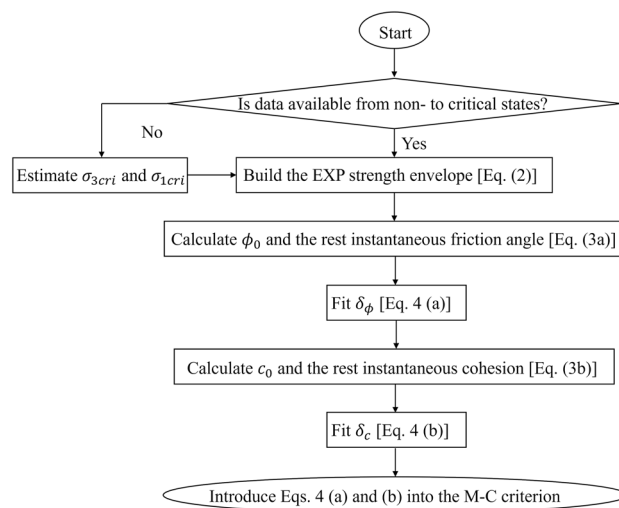


Figure 5. The procedural workflow for incorporating the SFC model.

in Fig. 3. Moreover, it is observed that the confining pressure of jointed rock masses at the critical state approximately aligns with its uniaxial compressive strength. This suggests that the stress-dependent friction angle and cohesion proposed in this study hold the potential for application to rock masses and engineering-scale problems. Therefore, future endeavors aim to express the stress-dependent shear parameters for rock masses as a function of the rock mass quality, as defined by the Rock Mass Rating (RMR) or Q rating.

Discussion: parameter (δ_ϕ and δ_c) sensitivity and their physical meaning

Parameter sensitivity of δ_ϕ and δ_c

Section “Model verification” demonstrates that the SFC model allows the M-C criterion to capture nonlinear strength responses across different rock types. The second advantage of the SFC model is its ability to project nonlinear strength across states from non-critical to critical by utilizing parameters derived from triaxial data at low confining pressure. This section focuses on proving and examining this advantage.

The SFC model has five parameters, i.e., δ_ϕ , δ_c , ϕ_0 , c_0 and c_{crit} . ϕ_0 and c_0 are calculated from test data, while c_{crit} is determined by the strength at the critical state. Only δ_ϕ and δ_c require fitting with test data. The insensitivity of δ_ϕ and δ_c to the range of σ_3 data used for fitting is the underlying principle behind the second advantage. This section will prove this statement. Additionally, a comparison of the sensitivity of δ_ϕ and δ_c with parameters in classical M-C and H-B criteria is provided to demonstrate the model’s superiority.

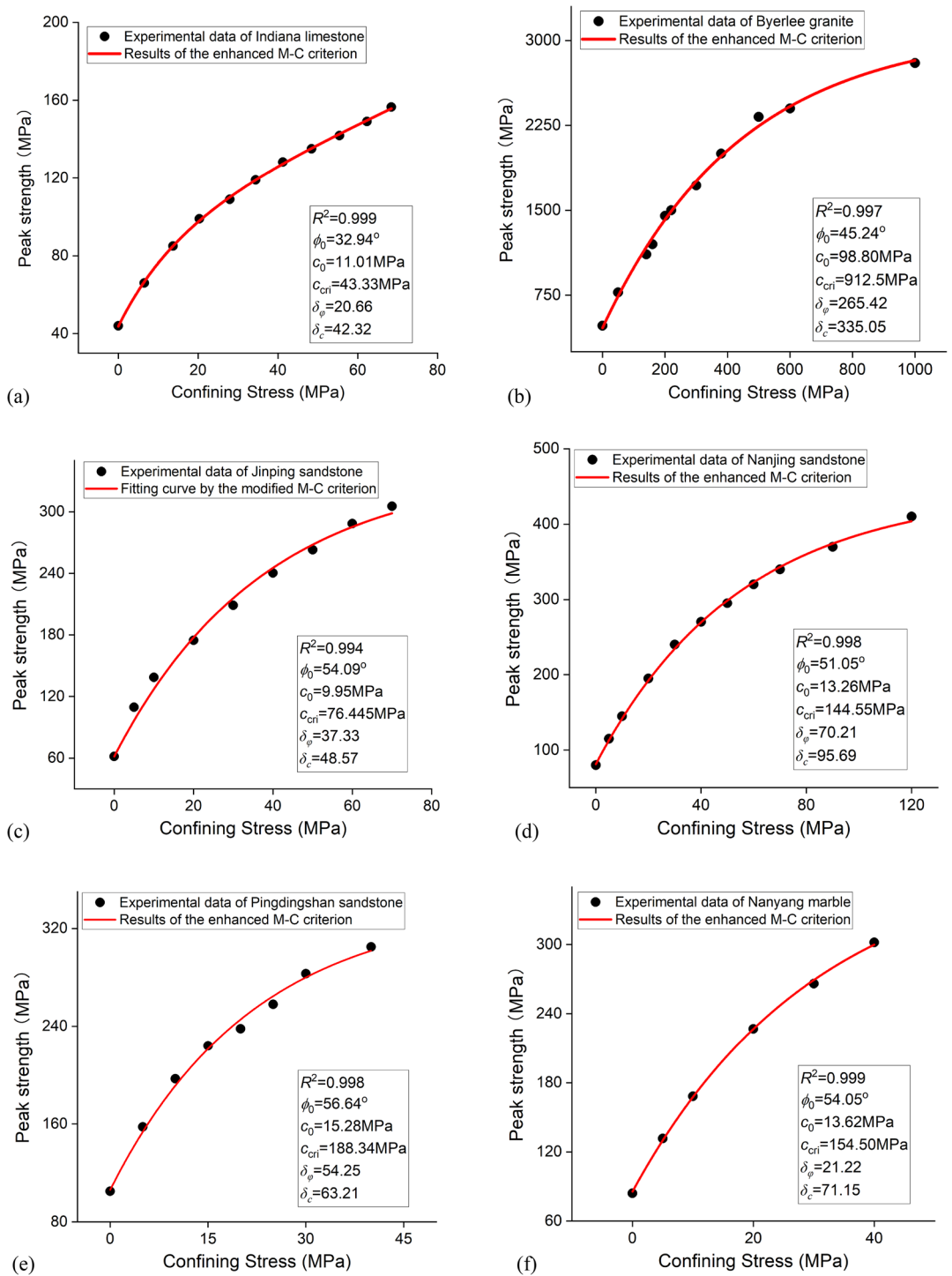


Figure 6. Comparison of fitting by the enhanced M-C criterion (red solid line) and experimental data from Table 2 (black points). (a) Indiana limestone from Ref.⁵³; (b) Byerlee granite⁵⁷; (c) Jinping sandstone⁵⁴; (d) Nanjing sandstone⁴³; (e) Pingdingshan sandstone⁹; (f) Nanyang marble⁹; (g) Jinyunshan Limestone; (h) Dunham dolomite⁵⁵; (i) Yamaguchi marble³²; (j) Dun Mountain dunite⁵⁶. (k) Jinyun sandstone. (l) Solnhofen limestone. (m) Dazhi marble. (n) Shanxi mudstone.

The H-B criterion for the intact rock is expressed as:

$$\sigma_1 = \sigma_3 + \sigma_{ci} \left(m_i \frac{\sigma_3}{\sigma_{ci}} + 1 \right)^{1/2} \tag{5}$$

where m_i is the parameter of the criterion. σ_{ci} is the UCS. Note that both m_i and σ_{ci} are fitted.

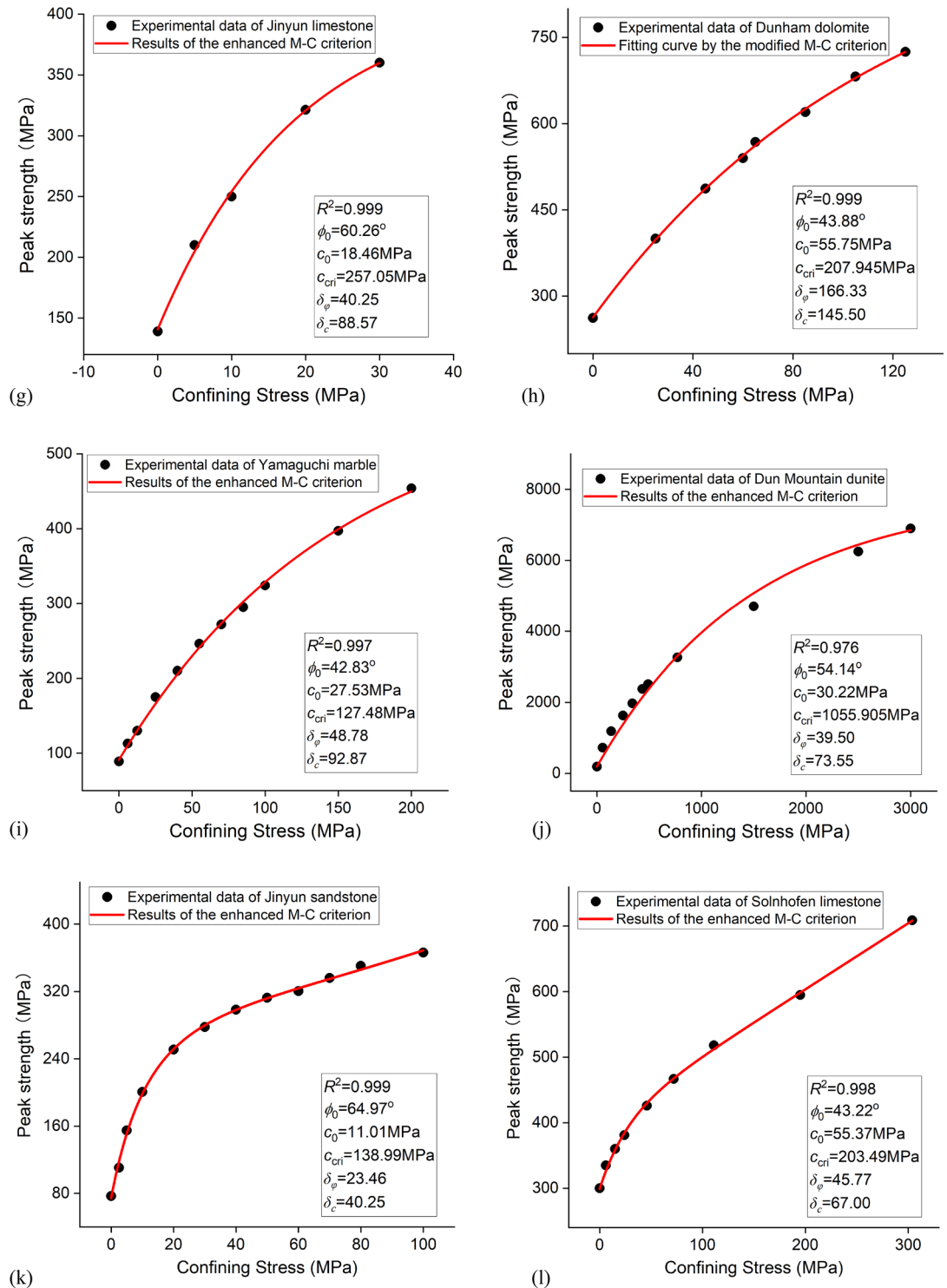


Figure 6. (continued)

The test data of limestone in Indiana in Table 2 is employed in this discussion. The parameters of the strength criteria (i.e., the classical M-C, SFC-enhanced M-C, and classical H-B criteria) for Indiana limestone are determined using the following methods: (1) utilizing the first three experimental data points, (2) utilizing the first four data points, and (3) considering subsequent ones as confining pressures increase, and finally (4) using all data points. The criterion parameters obtained are listed in Table 3.

It can be seen in Table 3 that there is a large variation of the parameters in the classical M-C and H-B criteria when different data points are employed. The standard deviations are 3.60 and 6.03 for ϕ and c , and 1.43 and 5.90 for m_i and σ_{ci} . This indicates that the parameters of the classical criteria are sensitive to the data cover range of σ_3 used in the best-fitting process. On the other hand, the parameters δ_ϕ and δ_c in the SFC model are insensitive to

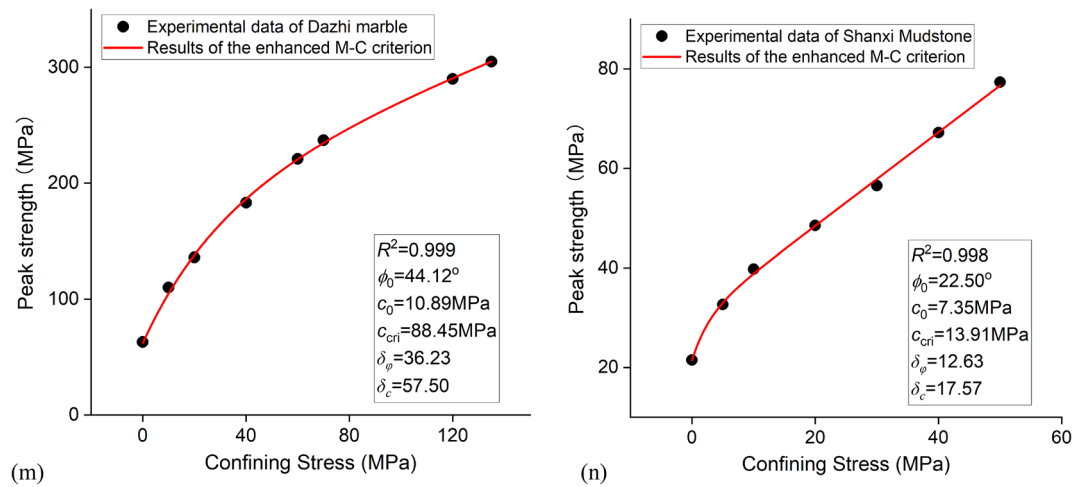


Figure 6. (continued)

Number of triaxial test data points used for fitting	Classical M-C criterion		Classical H-B criterion		Enhanced M-C criterion	
	$\phi(o)$	c (MPa)	m_i	σ_{ci} (MPa)	$\delta\phi$	δ_c
3	12.92	29.95	5.15	44.49	23.24	39.42
4	13.91	27.51	4.62	45.35	22.30	40.48
5	15.54	24.11	3.50	48.23	21.35	41.50
6	16.79	21.72	2.96	50.27	20.40	42.55
7	18.02	19.73	2.53	52.15	20.44	42.32
8	19.32	17.64	2.06	54.63	20.50	42.97
9	20.84	15.67	1.66	57.02	20.59	42.32
10	22.15	14.02	1.42	59.10	20.64	42.32
11	23.24	12.72	1.22	60.65	20.66	42.32
Standard deviation	3.60	6.03	1.43	5.90	0.92	1.08

Table 3. Parameters of the classical M-C, H-B and the enhanced M-C criteria fitted by a different range of confining stress.

the data points used in fitting, as their standard deviations are only 0.92 and 1.08, respectively. Correspondingly, the predictions and precision of classical criteria exhibit significant variability with different ranges of σ_3 used to determine their parameters, whereas the enhanced criteria with the SFC model do not. To substantiate this assertion, we utilize the parameters presented in Table 3. The strength responses predicted by the classical M-C, SFC-enhanced M-C, and classical H-B criteria are compared and depicted in Fig. 7. Figure 7a shows that the M-C criterion highly overpredicts the strength if it uses the parameters fitted by only the triaxial test data at lower σ_3 . More specifically, at $\sigma_3 = 68.4$ MPa, an overestimation of peak strength of 56.25%, 31.25%, 17.25%, 6.85%, and 6.25% is observed when three, five, seven, nine, and eleven data points are used, respectively. Figure 7b shows that the H-B criterion also highly overpredicts the strength if it only uses the parameters fitted by the test data at lower σ_3 . More specifically, at $\sigma_3 = 68.4$ MPa, an overestimation of peak strength of 28.84%, 19.23%, 12.82%, 7.69%, and 3.21% is observed when three, five, seven, nine, and eleven data points are used, respectively. On the other hand, results from the SFC-enhanced M-C criterion are closely aligned with the experimental data, no matter how many data points are used in parameter fitting (see Fig. 7c).

To further objectively assess the performance of the SFC-enhanced M-C criterion, results from the classical M-C, SFC-enhanced M-C, and classical H-B criteria are compared using index R^2 , error percentage (D_{ri}), mean absolute percentage error (MAPE, E_{aar}) and root-mean-square deviation (RMSD, E_{rms}). For our case (strength prediction), D_{ri} can indicate whether the criterion overpredicts or underpredicts rock strength. The negative D_{ri} mean underestimation and vice versa. The E_{rms} can reveal the variance of the prediction. Smaller D_{ri} , E_{aar} and E_{rms} indicate better performance. These error measurements are given in the following equation:

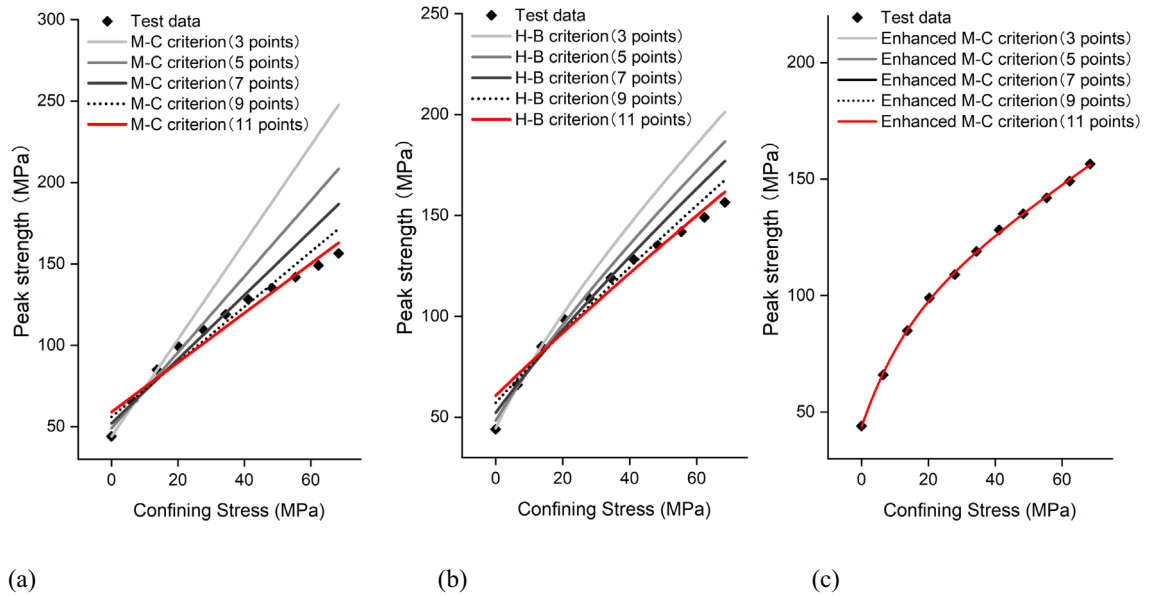


Figure 7. Comparison of experimental data and predicted results using different criteria. Rock specimen: Indiana limestone⁵³. (a) Conventional linear M-C criterion; (b) H-B criterion; (c) Enhanced M-C criterion. Note that values of the parameters in this three criteria are presented in Table 3 and Fig. 6a.

$$\begin{cases} D_{ri} = \frac{\sigma_{1,pre} - \sigma_{1,test}}{\sigma_{1,test}} \\ E_{aar} = \frac{\sum_{i=1}^N |D_{ri}|}{N} \\ E_{rms} = \sqrt{\frac{\sum_{i=1}^N (\sigma_{1,pre} - \sigma_{1,test})^2}{N}} \\ R^2 = 1 - \frac{\sum_{i=1}^N (\sigma_{1,pre} - \sigma_{1,test})^2}{\sum_{i=1}^N (\sigma_{1,test} - \sigma_{1,ave})^2} \end{cases} \quad (6)$$

where $\sigma_{1,pre}$ and $\sigma_{1,test}$ are the result from the criterion and experimental test, respectively; N is the number of test; $\sigma_{1,ave}$ is the average of all testing values.

Using the parameters in Table 3, the evaluation metrics (i.e., Eq. (6)) of the three criteria are summarized in Table 4. Combining Tables 3, 4, and Fig. 7 indicates that: (1) The parameters δ_ϕ and δ_c of the SFC model are insensitive to the data points and range of σ_3 employed for fitting. This indicates that δ_ϕ and δ_c obtained from triaxial data at a low σ_3 range can be used to determine rock strength at a higher σ_3 . (2) The accuracy of the classical M-C and H-B criteria depends on the range of σ_3 used to determine their parameters. Extensive triaxial testing across a wide range of σ_3 is necessary for parameter fitting and increased accuracy when applying the classical criteria. This process can be resource-intensive, particularly for hard rocks with high $\sigma_{3,cri}$. Correspondingly, the H-B envelope fitted with triaxial data at low σ_3 may result in inaccuracies in Balmer’s and Hoek’s method for determining the equivalent friction angle and cohesion. (3) When the data of the whole range of σ_3 is used for parameter fitting (i.e., 11 points), the SFC-enhanced M-C criterion outperforms the classical criteria. Table 4 indicates that the enhanced M-C criterion outperforms the classical criteria, showing lower MAPE and RMSD, as well as higher R^2 values. As shown in Fig. 6, the classical criteria overestimate the UCS and the strength at

Number of test data used for fitting	Classical M-C criterion			Classical H-B criterion			Enhanced M-C criterion		
	R^2	RMSE/MPa	AAEP/%	R^2	RMSE/MPa	AAEP/%	R^2	RMSE/MPa	AAEP/%
3	0.355	28.79	15.77	0.434	25.60	14.19	0.998	2.02	1.04
4	0.436	25.59	14.22	0.477	24.87	12.74	0.9986	2.01	1.04
5	0.483	22.45	12.67	0.501	24.03	9.85	0.998	1.89	0.88
6	0.696	18.73	10.62	0.874	12.71	7.52	0.999	1.36	0.80
7	0.824	13.32	9.72	0.913	10.03	7.45	0.999	1.28	0.55
8	0.875	11.52	8.55	0.927	9.15	7.37	0.999	1.22	0.52
9	0.938	8.44	7.49	0.930	8.21	7.35	0.999	1.20	0.50
10	0.945	8.01	7.22	0.955	7.12	7.29	0.999	1.20	0.50
11	0.955	7.19	7.17	0.9611	6.70	7.21	0.999	1.20	0.50

Table 4. Prediction accuracy analysis of the classical M-C, H-B and the enhanced M-C criteria fitted by a different range of confining stress.

higher σ_3 . They also underestimate the strength at moderate σ_3 . This indicates that when data spanning from non-critical to the critical state is available, Balmer's and Hoek's methods for determining the equivalent friction angle and cohesion may also be inaccurate due to their original Hoek–Brown (H-B) strength envelope not aligning with the strength responses of rocks.

Please note that the conclusions drawn above are not specific to any particular case; rather, they represent universal findings applicable to a wide range of rocks, including those listed in Tables 1 and 2. In scenarios where researchers are constrained by test equipment and experimental conditions, they may only obtain test data at lower confining pressures preceding the critical state. In such situations, we recommend acquiring data within a range of confining pressures equal to at least 40% of the critical confining pressure (i.e., the UCS) and subsequently applying the process outlined in Fig. 5 of the article to implement the enhanced M-C criterion, thereby ensuring precise strength predictions. However, it's important to acknowledge that the SFC-enhanced M-C criterion also has limitations, particularly concerning the empirical estimation of confining pressure and strength at the critical state. While the empirical method employed to estimate these parameters in this article is considered relatively accurate by many scholars^{7,8,17,40}, it's essential to recognize that the confining pressure and strength at the critical state may vary depending on internal factors, such as mineral composition, grain size and shape, and porosity. Further research is warranted to investigate this aspect, and the development of mathematical models is necessary to accurately calculate the confining pressure and strength at the critical state.

Physical significance of δ_ϕ and δ_c

The SFC model has five parameters, i.e., δ_ϕ , δ_c , ϕ_0 , c_0 and c_{cri} . As discussed in sections “The stress-dependent cohesion (c_i) and friction angle (ϕ_i)” and “Model verification”, ϕ_0 and c_0 represent the initial friction angle and cohesion, respectively. c_{cri} denotes the maximum cohesion achievable after reaching the critical state. In the following part, we provide detailed insights into the physical interpretations of the parameters δ_ϕ and δ_c . Parameters δ_ϕ and δ_c are crucial in shaping the ϕ_i and c_i curves. As illustrated in Fig. 8a, a smaller value of δ_ϕ results in a higher slope and curvature of the stress-dependent friction angle curve, indicative of a more rapid decrease rate with increasing confining pressure. Similarly, in Fig. 8b, a smaller value of δ_c leads to a higher slope and curvature

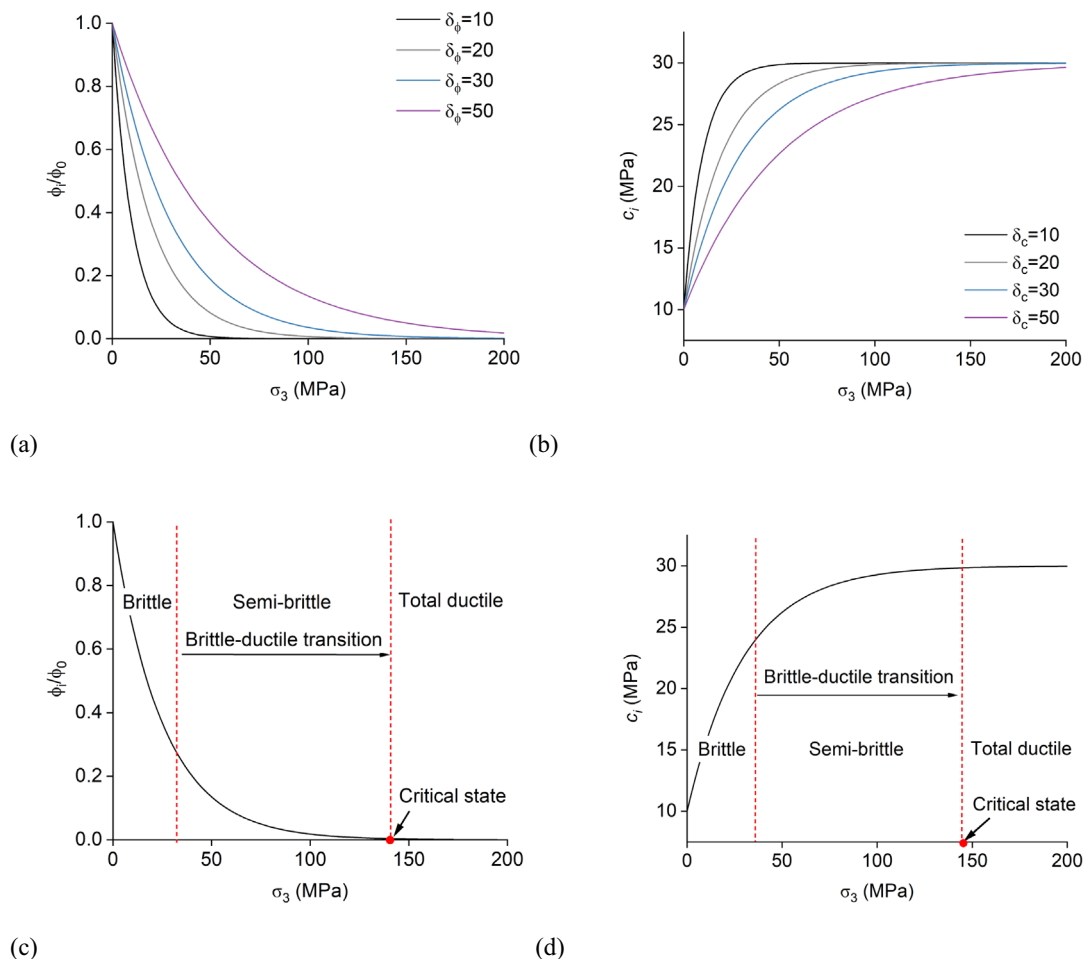


Figure 8. Parameter significance. (a) Influence of δ_ϕ on the stress-dependent friction angle curve under various σ_3 . (b) Influence of δ_c on the stress-dependent cohesion curve under various σ_3 . ($c_0 = 10$ MPa, $c_u = 30$ MPa).

of the stress-dependent cohesion curve, corresponding to a more rapid increase rate with elevated confining pressure. Fundamentally, as analysed in section “The stress-dependent cohesion (c_i) and friction angle (ϕ_i)”, the mobilization of ϕ_i and c_i under increased σ_3 is attributed to the rock undergoing a brittle-ductile transition as σ_3 rises (see Fig. 8c,d). Notably, the span of σ_3 from non-critical to the critical state also increases with the rise of δ_ϕ and δ_c (see Fig. 8a,b). Therefore, based on the above discussion, we can conclude that δ_ϕ and δ_c essentially serve as material constants reflecting the ability of the rock to sustain brittle behavior across different loading conditions. The higher the value of δ_ϕ and δ_c , the higher the σ_3 at the critical state, and the larger the range of σ_3 for the brittle-ductile transition of the rock. In other words, the rock with higher δ_ϕ and δ_c can still exhibit brittle characteristics under high σ_3 conditions.

Different types of rocks may exhibit variations in their ability to maintain brittleness under elevated confining pressures, resulting in distinct values for δ_ϕ and δ_c . This prompts a relevant question: Why do rocks exhibit varied brittleness durability, resulting in different curvatures of the ϕ_i and c_i curves and different spans of non-critical to critical states?

The answer lies in the compressibility of the solid rock skeleton, which refers to its ability to deform appropriately under external loads, preventing internal pore collapse and inducing deformation such as closure and shear sliding, leading to crack initiation and propagation. In the brittle and semi-brittle regions, the failure process of rocks under external loads is governed by crack development. This process involves pre-existing micropore compaction, micropore face interlocking, sliding movement caused by the breakage of irregularities on the pore surface, first crack initiation, propagation, and interaction with other initiated cracks to form macrocracks. Subsequently, a macroscopic crack development cycle occurs: macrocrack compaction, sliding, new crack initiation and connection, leading to the final formation of macro ruptures. From the preceding analysis in section “The stress-dependent cohesion (c_i) and friction angle (ϕ_i)”, it becomes evident that the mechanical response of rocks in brittle and semi-brittle regions is intricately linked to the closure and sliding resistance of the micropores and macrocracks. When σ_3 surpasses the critical state, the pores inside the rock do not compress to close. Instead, the overwhelming pressure transmitted from all directions directly crushes the pores, resulting in compactive cataclastic flow⁵⁸. Based on this foundation, the distinct brittleness durability exhibited by rocks, leading to unique curves for the stress-dependent friction angle and cohesion, is attributed to variations in the compressibility of their skeleton. Rocks with higher compressibility exhibit closure and deformation of internal pores under high pre-set hydrostatic pressures, facilitating later crack initiation and macro rupture formation, leading to higher brittleness durability. In contrast, rocks with lower compressibility do not deform and compress their internal pores even under low pre-set hydrostatic pressures. Instead, they undergo direct collapse and compactive cataclastic flow under external pressure, resulting in low brittleness durability.

Conclusions

In this paper, an innovative SFC is introduced in the M-C criterion to capture the nonlinear strength envelope. This approach involves a novel method for determining ϕ_i and c_i at each corresponding σ_3 , leading to the derivation of the SFC model. The SFC-enhanced M-C criterion, utilizing parameters obtained from triaxial tests under lower σ_3 , demonstrates the capability to delineate the complete non-linear strength envelope in (σ_1, σ_3) space, spanning from brittle to ductile behavior. Drawing from rock failure mechanisms spanning from the microscopic to macroscopic scales, we analyze the softening and hardening behaviors of ϕ_i and c_i . Additionally, the physical significance of parameters in the SFC model has been discussed. Validated through triaxial tests conducted on various rocks, the results indicate the SFC-enhanced criterion works well across these rocks.

Data availability

All data generated or analysed during this study are included in this published article.

Received: 26 March 2024; Accepted: 19 July 2024

Published online: 29 July 2024

References

1. Brady, B. H. & Brown, E. T. *Rock Mechanics: For Underground Mining* (Springer Science & Business Media, 2013).
2. Cai, W. *et al.* Three-dimensional forward analysis and real-time design of deep tunneling based on digital in-situ testing. *Int. J. Mech. Sci.* **226**, 107385. <https://doi.org/10.1016/j.ijmecsci.2022.107385> (2022).
3. Ranjith, P. G. *et al.* Opportunities and challenges in deep mining: A brief review. *Engineering* **3**, 546–551. <https://doi.org/10.1016/J.ENG.2017.04.024> (2017).
4. Fairhurst, C. Some challenges of deep mining. *Engineering* **3**, 527–537. <https://doi.org/10.1016/J.ENG.2017.04.017> (2017).
5. Gibowicz, S. J. & Kijko, A. *An Introduction to Mining Seismology* (Elsevier, 2013).
6. Mogi, K. Pressure dependence of rock strength and transition from brittle fracture to ductile flow. *Bull. Earthq. Res. Inst.* **44**, 215–232 (1966).
7. Barton, N. The shear strength of rock and rock joints. *Int. J. Rock Mech. Min. Sci. Geomech. Abstr.* **13**, 255–279. [https://doi.org/10.1016/0148-9062\(76\)90003-6](https://doi.org/10.1016/0148-9062(76)90003-6) (1976).
8. Barton, N. Shear strength criteria for rock, rock joints, rockfill and rock masses: Problems and some solutions. *J. Rock Mech. Geotech. Eng.* **5**, 249–261. <https://doi.org/10.1016/j.jrmge.2013.05.008> (2013).
9. You, M. Mechanical characteristics of the exponential strength criterion under conventional triaxial stresses. *Int. J. Rock Mech. Min. Sci.* **47**, 195–204 (2010).
10. Singh, M. & Singh, B. A strength criterion based on critical state mechanics for intact rocks. *Rock Mech. Rock Eng.* **38**, 243–248. <https://doi.org/10.1007/s00603-004-0042-3> (2005).
11. Sari, M. An improved method of fitting experimental data to the Hoek-Brown failure criterion. *Eng. Geol.* **127**, 27–35. <https://doi.org/10.1016/j.enggeo.2011.12.011> (2012).
12. Hobbs, D. W. The behavior of broken rock under triaxial compression. *Int. J. Rock Mech. Min. Sci. Geomech. Abstr.* **7**, 125–148. [https://doi.org/10.1016/0148-9062\(70\)90008-2](https://doi.org/10.1016/0148-9062(70)90008-2) (1970).

13. Sheorey, P. R., Biswas, A. K. & Choubey, V. D. An empirical failure criterion for rocks and jointed rock masses. *Eng. Geol.* **26**, 141–159. [https://doi.org/10.1016/0013-7952\(89\)90003-3](https://doi.org/10.1016/0013-7952(89)90003-3) (1989).
14. Qu, R. T. & Zhang, Z. F. A universal fracture criterion for high-strength materials. *Sci. Rep.* **3**, 1117. <https://doi.org/10.1038/srep01117> (2013).
15. Li, Y. *et al.* Strength criterion of rock mass considering the damage and effect of joint dip angle. *Sci. Rep.* **12**, 2601. <https://doi.org/10.1038/s41598-022-06317-1> (2022).
16. Xie, S.-J., Lin, H., Chen, Y.-F. & Wang, Y.-X. A new nonlinear empirical strength criterion for rocks under conventional triaxial compression. *J. Central South Univ.* **28**, 1448–1458. <https://doi.org/10.1007/s11771-021-4708-8> (2021).
17. Singh, M., Raj, A. & Singh, B. Modified Mohr-Coulomb criterion for non-linear triaxial and polyaxial strength of intact rocks. *Int. J. Rock Mech. Min. Sci.* **48**, 546–555. <https://doi.org/10.1016/j.ijrmms.2011.02.004> (2011).
18. Balmer, G. A general analysis solution for Mohr's envelope. *Proceedings of American Society of Test Materials* **52**, 1260–1271 (1952).
19. Hoek, E. & Brown, E. T. Empirical strength criterion for rock masses. *J. Geotech. Eng. Div.* **106**, 1013–1035 (1980).
20. Lee, Y.-K. & Pietruszczak, S. Analytical representation of Mohr failure envelope approximating the generalized Hoek-Brown failure criterion. *Int. J. Rock Mech. Min. Sci.* **100**, 90–99. <https://doi.org/10.1016/j.ijrmms.2017.10.021> (2017).
21. Hoek, E. in *International Journal of Rock Mechanics and Mining Sciences & Geomechanics Abstracts*. 227–229 (Elsevier BV).
22. Yang, X.-L. & Yin, J.-H. Linear Mohr-Coulomb strength parameters from the non-linear Hoek-Brown rock masses. *Int. J. Non-Linear Mech.* **41**, 1000–1005 (2006).
23. Yang, X.-L. & Yin, J.-H. Slope equivalent Mohr-Coulomb strength parameters for rock masses satisfying the Hoek-Brown criterion. *Rock Mech. Rock Eng.* **43**, 505–511 (2010).
24. Shen, J., Priest, S. & Karakus, M. Determination of Mohr-Coulomb shear strength parameters from generalized Hoek-Brown criterion for slope stability analysis. *Rock Mech. Rock Eng.* **45**, 123–129 (2012).
25. Sofianos, A. & Halakatevakis, N. Equivalent tunnelling Mohr-Coulomb strength parameters for given Hoek-Brown ones. *Int. J. Rock Mech. Min. Sci.* **1997**(39), 131–137 (2002).
26. Zhang, F.-P., Li, D.-Q., Cao, Z.-J., Xiao, T. & Zhao, J. Revisiting statistical correlation between Mohr-Coulomb shear strength parameters of Hoek-Brown rock masses. *Tunn. Undergr. Space Technol.* **77**, 36–44 (2018).
27. Rukhaiyar, S. & Samadhiya, N. K. Triaxial strength behaviour of rockmass satisfying Modified Mohr-Coulomb and generalized Hoek-Brown criteria. *Int. J. Min. Sci. Technol.* **28**, 901–915 (2018).
28. Song, Y., Feng, M. & Chen, P. Modified minimum principal stress estimation formula based on Hoek-Brown criterion and equivalent Mohr-Coulomb strength parameters. *Sci. Rep.* **13**, 6409. <https://doi.org/10.1038/s41598-023-33053-x> (2023).
29. Hoek, E., Carranza-Torres, C. & Corkum, B. Hoek-Brown failure criterion-2002 edition. *Proc. NARMS-Tac 1*, 267–273 (2002).
30. Walton, G. A new perspective on the brittle-ductile transition of rocks. *Rock Mech. Rock Eng.* **54**, 5993–6006 (2021).
31. Byerlee, J. D. Frictional characteristics of granite under high confining pressure. *J. Geophys. Res.* **72**, 3639–3648 (1967).
32. Mogi, K. *Experimental Rock Mechanics* (CRC Press, 2006).
33. Lin, Z. Y., Wu, Y. S. & Guan, L. L. Research on the brittle-ductile transition property of rocks under triaxial compression (in Chinese). *Rock Soil Mech.* **13**, 45–53 (1992).
34. Lu, Y., Wang, L., Yang, F., Li, Y.-J. & Chen, H.-M. Post-peak strain softening mechanical properties of weak rock. *Chin. J. Rock Mech. Eng.* **29**, 640–648 (2010).
35. Liu, H., Cui, S., Meng, Y., Chen, Z. & Sun, H. Study on mechanical properties and wellbore stability of deep sandstone rock based on variable parameter MC criterion. *Geoenergy Sci. Eng.* **224**, 211609 (2023).
36. Wang, Y.-N., Wang, L.-C. & Zhou, H.-Z. An experimental investigation and mechanical modeling of the combined action of confining stress and plastic strain in a rock mass. *Bull. Eng. Geol. Environ.* **81**, 204 (2022).
37. Gentzis, T., Deisman, N. & Chalaturnyk, R. J. Geomechanical properties and permeability of coals from the Foothills and Mountain regions of western Canada. *Int. J. Coal Geol.* **69**, 153–164 (2007).
38. Yang, Y., Lai, Y. & Chang, X. Laboratory and theoretical investigations on the deformation and strength behaviors of artificial frozen soil. *Cold Regions Sci. Technol.* **64**, 39–45 (2010).
39. Wang, S. *et al.* A universal method for quantitatively evaluating rock brittle-ductile transition behaviors. *J. Pet. Sci. Eng.* **195**, 107774. <https://doi.org/10.1016/j.petrol.2020.107774> (2020).
40. Shen, B., Shi, J. & Barton, N. An approximate nonlinear modified Mohr-Coulomb shear strength criterion with critical state for intact rocks. *J. Rock Mech. Geotech. Eng.* **10**, 645–652. <https://doi.org/10.1016/j.jrmge.2018.04.002> (2018).
41. You, M. Comparison of the accuracy of some conventional triaxial strength criteria for intact rock. *Int. J. Rock Mech. Min. Sci.* **48**, 852–863 (2011).
42. Byerlee, J. D. Brittle-ductile transition in rocks. *J. Geophys. Res.* **73**, 4741–4750 (1968).
43. Liu, S.-L., Chen, H.-R., Yuan, S.-S. & Zhu, Q.-Z. Experimental investigation and micromechanical modeling of the brittle-ductile transition behaviors in low-porosity sandstone. *Int. J. Mech. Sci.* **179**, 105654 (2020).
44. Ulusay, R. *The ISRM Suggested Methods for Rock Characterization, Testing and Monitoring: 2007–2014*. (2015).
45. Wolberg, J. *Data Analysis Using the Method of Least Squares: Extracting the Most Information from Experiments* (Springer Science & Business Media, 2006).
46. Hoek, E. & Brown, E. T. The Hoek-Brown failure criterion and GSI—2018 edition. *J. Rock Mech. Geotech. Eng.* **11**, 445–463. <https://doi.org/10.1016/j.jrmge.2018.08.001> (2019).
47. Rudnicki, J. W. & Rice, J. Conditions for the localization of deformation in pressure-sensitive dilatant materials. *J. Mech. Phys. Solids* **23**, 371–394 (1975).
48. Li, H., Zhong, R., Pel, L., Smeulders, D. & You, Z. A new volumetric strain-based method for determining the crack initiation threshold of rocks under compression. *Rock Mech. Rock Eng.* **57**, 1329–1351. <https://doi.org/10.1007/s00603-023-03619-2> (2024).
49. Li, H., Pel, L., You, Z. & Smeulders, D. Enhanced Hoek-Brown (H-B) criterion incorporating kinetic porosity-dependent instantaneous m_i for rocks exposed to chemical corrosion. *Int. J. Min. Sci. Technol.* <https://doi.org/10.1016/j.ijmst.2024.05.002> (2024).
50. Zhu, S. *et al.* An analytical model for pore volume compressibility of reservoir rock. *Fuel* **232**, 543–549. <https://doi.org/10.1016/j.fuel.2018.05.165> (2018).
51. Peng, S. & Johnson, A. in *International Journal of Rock Mechanics and Mining Sciences & Geomechanics Abstracts*. 37–86 (Elsevier).
52. Wu, Z. & Wong, L. N. Y. Frictional crack initiation and propagation analysis using the numerical manifold method. *Comput. Geotech.* **39**, 38–53. <https://doi.org/10.1016/j.compgeo.2011.08.011> (2012).
53. Hoek, E. Strength of jointed rock masses. *Geotechnique* **33**, 187–223 (1983).
54. You, M. Three independent parameters to describe conventional triaxial compressive strength of intact rocks. *J. Rock Mech. Geotech. Eng.* **2**, 350–356 (2010).
55. Mogi, K. On the pressure dependence of strength of rocks and the coulomb fracture criterion. *Tectonophysics* **21**, 273–285. [https://doi.org/10.1016/0040-1951\(74\)90055-9](https://doi.org/10.1016/0040-1951(74)90055-9) (1974).
56. Shimada, M., Cho, A. & Yukutake, H. Fracture strength of dry silicate rocks at high confining pressures and activity of acoustic emission. *Tectonophysics* **96**, 159–172. [https://doi.org/10.1016/0040-1951\(83\)90248-2](https://doi.org/10.1016/0040-1951(83)90248-2) (1983).
57. Paterson, M. S. & Wong, T.-F. *Experimental Rock Deformation: The Brittle Field* Vol. 348 (Springer, 2005).
58. Wong, T.-F. & Baud, P. The brittle-ductile transition in porous rock: A review. *J. Struct. Geol.* **44**, 25–53 (2012).

Acknowledgements

The authors wish to thank Dr. Xiaohong Zhu for useful suggestions and discussion. Special thanks to Prof. Liangqi Zhang and Prof. Keshui Ge for their help, passion and enthusiasm devoted to this scientific investigation.

Author contributions

H.L.: Conceptualization; Methodology; Investigation; Formal analysis; Writing. L.P.: Supervision; Review and editing. Z.Y.: Supervision; Formal analysis; Review and editing. D.S.: Supervision; Project administration; Review and editing.

Competing interests

The authors declare no competing interests.

Additional information

Correspondence and requests for materials should be addressed to H.L. or L.P.

Reprints and permissions information is available at www.nature.com/reprints.

Publisher's note Springer Nature remains neutral with regard to jurisdictional claims in published maps and institutional affiliations.



Open Access This article is licensed under a Creative Commons Attribution-NonCommercial-NoDerivatives 4.0 International License, which permits any non-commercial use, sharing, distribution and reproduction in any medium or format, as long as you give appropriate credit to the original author(s) and the source, provide a link to the Creative Commons licence, and indicate if you modified the licensed material. You do not have permission under this licence to share adapted material derived from this article or parts of it. The images or other third party material in this article are included in the article's Creative Commons licence, unless indicated otherwise in a credit line to the material. If material is not included in the article's Creative Commons licence and your intended use is not permitted by statutory regulation or exceeds the permitted use, you will need to obtain permission directly from the copyright holder. To view a copy of this licence, visit <http://creativecommons.org/licenses/by-nc-nd/4.0/>.

© The Author(s) 2024